Independence of plasmonic near-field enhancements to illumination beam profile

Matthew R. Foreman*
Blackett Laboratory, Department of Physics, Imperial College London, Prince Consort Road, London, SW7 2AZ, United Kingdom

Yonatan Sivan
Blackett Laboratory, Department of Physics, Imperial College London, Prince Consort Road, London, SW7 2AZ, United Kingdom and Complex Photonic Systems, Faculty of Science and Technology, and MESA + Institute for Nanotechnology, University of Twente, P.O. Box 217, 7500 AE Enschede, The Netherlands

Stefan A. Maier and Peter Török
Blackett Laboratory, Department of Physics, Imperial College London, Prince Consort Road, London, SW7 2AZ, United Kingdom
(Received 29 August 2012; published 22 October 2012)

Near-field enhancements of the electric field at the center of spheroidal multilayer metallic nanoparticles (NPs) are investigated when illuminated by focused beams of arbitrary field structure (i.e., amplitude, phase, and polarization distributions). Employing a Mie-type representation, the enhancement at the center of such NPs (such as a core-shell geometry) is analytically shown to be independent of the field structure of the illumination beam for both on- and off-axis NPs. Furthermore, it is shown that, to leading order, the average field enhancement in the near field of these NPs is also approximately illumination independent.

DOI: 10.1103/PhysRevB.86.155441 PACS number(s): 78.67.Bf, 87.64.M−, 73.20.Mf, 42.25.Bs

I. INTRODUCTION

Metallic nanoparticles (NPs) enable concentration of an electromagnetic field in regions smaller than allowed by diffraction. These regions contain field amplitudes that can be significantly higher than the incident field. This property opens the way to various applications such as single molecule spectroscopy, biosensing, absorption enhancement in solar cells, improved drug delivery, as well as to improving signal intensity in fluorescence microscopy (see, e.g., Ref. 1 and references therein). Recently, it has also been proposed to exploit this plasmonic near-field enhancement in order to improve performance in various far-field super-resolution techniques such as structured illumination microscopy (SIM)[2–4] and stimulated-emission-depletion (STED) microscopy[5–9] (see Ref. 10 for a recent review).

Quantitative knowledge of the near-field enhancement levels achievable by use of NPs is important in such applications. Studies of this kind usually employ either quasistatic approximations, Mie-type solutions, or rigorous numerical calculations, yet are performed almost always under the assumption of a linearly polarized plane-wave illumination (i.e., a spatially uniform intensity, polarization and phase distribution illuminating the NP). When metallic NPs are used in standard wide-field microscopy techniques, the assumption of a plane-wave illumination is well justified. However, there are many configurations where the illumination can be nonuniform. For example, scanning microscopy (both near and far field) uses strongly localized beams, such that when the illumination beam is shifted away from the NP center (or vice versa), nonuniform fields are incident upon the NP. Moreover, in modern microscopy, wide-field techniques such as structured illumination[2–4] and HiLo sectioning,[11] as well as scanning techniques such as STED microscopy,[5–7] employ complex illumination patterns which can exhibit subwavelength variations (shown schematically in Fig. 1). Going beyond applications in microscopy, complex illumination patterns such as Laguerre-Gaussian (LG) beams,[12,13] "dark spot" beams,[14] cylindrically polarized beams,[15–17] or even completely irregularly shaped beams[18] have been recently employed for selective mode and spot excitation in nanoplasmonic systems.

In order to obtain accurate results for field enhancements in all such cases, the actual illumination pattern must be taken into account. Accordingly a natural question arises regarding the illumination dependence of the field enhancement factor achievable by use of NPs. In particular, for a given NP configuration beam shapes producing optimal field enhancements are of interest, whereas in a scanning configuration the variation of field enhancement with scan position becomes a concern. The intent of this article is to address these, and related, questions. Despite the complexity of the problem, a very simple and generic result is derived for (multilayer) spheroidal NPs; namely, it is shown that at the core of such NPs the plasmonic enhancement factor is rigorously independent of the illumination profile used. This result is especially relevant in techniques assisted by metal (as well as dielectric) NPs,[8] as well as in nanolasing,[19] optical cloaking,[20] and other applications. Consideration of average enhancement factors near the surface of NPs is also considered here, and the conditions under which this can exhibit illumination independent behavior highlighted and discussed. This is pertinent to fluorescence microscopy in which NPs are coated with fluorophores, or random collections of NPs and fluorescent molecules are exploited.[21]

II. RESULTS AND DISCUSSION

A. Focusing and scattering formalism

Throughout this article a Mie-type (or multipole) solution to Maxwell's equations is adopted, because the quasistatic limit rapidly breaks down, even for NPs as small as ∼20 nm, and numerical calculations provide limited physical insight.

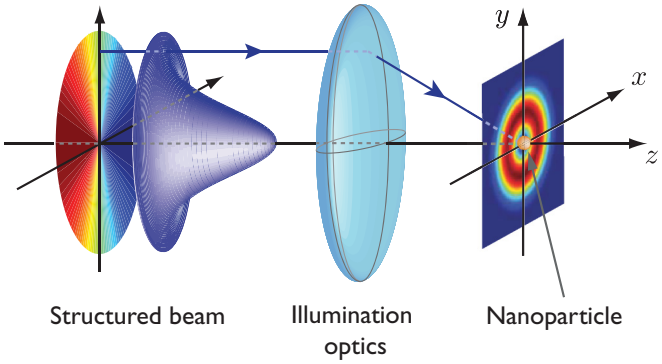

FIG. 1. (Color online) Schematic illustration of the focusing of a structured beam (e.g., a Gaussian beam with spiral phase) onto a nanoparticle.

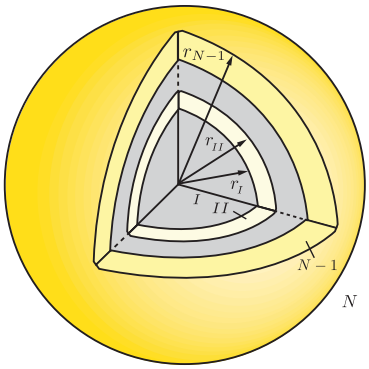

FIG. 2. (Color online) Schematic illustration of a multilayer nanoparticle, with distinct layers indexed as $I, II, \ldots N-1$, of respective radius $r_I, r_{II}, \ldots r_{N-1}$, immersed in a medium indexed as N.

Furthermore the setups discussed above typically operate by focusing of beams with arbitrary amplitude, phase, and polarization structure, a scenario which is highly amenable to a multipole description,[22,23] hence also motivating this approach.

Vectorial electric and magnetic multipoles represent a rigorous and complete solution to Maxwell's equations within isotropic media and can hence be used to represent the field in each of these regions. Particularly, it is first noted that an arbitrary electric field can be expressed in the form,

$$\mathbf{E}(\mathbf{r}) = \sum_{j}\sum_{\nu}\sum_{l,m} a_{lm}^{\nu(j)}\mathbf{E}_{lm}^{\nu(j)}(\mathbf{r}), \tag{1}$$

where, in terms of spherical components $(E_r, E_\vartheta, E_\varphi)$,

$$\mathbf{E}_{lm}^{E(j)}(\mathbf{r}) = \begin{bmatrix} l(l+1)\frac{h_l^{(j)}(kr)}{r}Y_l^m(\vartheta,\varphi) \\ \frac{1}{r}\frac{d}{dr}\left(rh_l^{(j)}(kr)\right)\frac{\partial}{\partial\vartheta}Y_l^m(\vartheta,\varphi) \\ \frac{im}{r\sin\vartheta}\frac{d}{dr}\left(rh_l^{(j)}(kr)\right)Y_l^m(\vartheta,\varphi) \end{bmatrix},$$

$$\mathbf{E}_{lm}^{M(j)}(\mathbf{r}) = \begin{bmatrix} 0 \\ \frac{ik_2m}{\sin\vartheta}h_l^{(j)}(kr)Y_l^m(\vartheta,\varphi) \\ -k_2h_l^{(j)}(kr)\frac{\partial}{\partial\vartheta}Y_l^m(\vartheta,\varphi) \end{bmatrix},$$

$a_{lm}^{\nu(j)}$ is the weighting coefficient for the multipole mode of order $l = 1,2,\ldots,$ and $m = -l, -l+1, \ldots, l$ and ν denotes either electric (E) or magnetic (M) multipoles. The multipole modes depend on the material properties via the constants $k_1 = i\omega\epsilon - \sigma/\omega$, $k_2 = i\omega\mu$, where $k^2 = -k_1k_2$, ϵ is the permittivity of the medium, μ is the permeability (assumed henceforth to be μ_0), and σ is the conductivity.[24] An $\exp(-i\omega t)$ time dependence has also been assumed. Furthermore, $Y_l^m(\vartheta,\varphi)$ are the spherical harmonics defined by $Y_l^m(\vartheta,\varphi) = C_{lm}P_l^{|m|}(\cos\vartheta)\exp(im\varphi)$, where $P_l^{|m|}(\cos\vartheta)$ are the associated Legendre polynomials, $h_l^{(j)}(kr)$ denotes the spherical Hankel $(j = 1,2)$ or spherical Bessel $(j = 3)$ functions, and $C_{lm} = ((2l+1)(l-|m|)!/4\pi(l+|m|)!)^{1/2}$. Physically, the $j = 1$ modes represent multipole sources, in which energy flows outward from $\mathbf{r} = \mathbf{0}$ while $j = 2$ represents field sinks with energy flowing inwards towards the sink position. In contrast, spherical Bessel functions constitute a superposition of both $j = 1$ and $j = 2$ in equal measure $(h_l^{(3)}(z) = [h_l^{(1)}(z) + h_l^{(2)}(z)]/2)$ and hence have finite energy density at the origin.

Given these observations, consider a multilayered NP with spherical symmetry with $N-1$ layers, where the inner core is denoted by index I and the layer index is incremented with increasing radius (see Fig. 2). Most notable (and practical) of such configurations is the two-layer shell-core NP,[25] or a single material homogeneous NP, however, all results derived are applicable to multilayer NPs. The NP is itself located in a medium which constitutes the N^{th} distinct region in the scattering problem. The field within each region can then be written,

$$\begin{aligned} \mathbf{E}^{I}(\mathbf{r}) &= \sum_{\nu}\sum_{l,m} c_{lm}^{\nu(3)}\mathbf{E}_{lm}^{\nu(3)}(\mathbf{r}), \\ \mathbf{E}^{II}(\mathbf{r}) &= \sum_{\nu}\sum_{l,m} d_{lm}^{\nu(2)}\mathbf{E}_{lm}^{\nu(2)}(\mathbf{r}) + e_{lm}^{\nu(1)}\mathbf{E}_{lm}^{\nu(1)}(\mathbf{r}), \\ &\vdots \\ \mathbf{E}^{N}(\mathbf{r}) &= \sum_{\nu}\sum_{l,m} a_{lm}^{\nu(3)}\mathbf{E}_{lm}^{\nu(3)}(\mathbf{r}) + b_{lm}^{\nu(1)}\mathbf{E}_{lm}^{\nu(1)}(\mathbf{r}), \end{aligned} \tag{2}$$

where it is noted that spherical Bessel functions $(j = 3)$ are used for both the illumination and the field within the NP core, so as ensure the field is well behaved at the origin and maintain physicality in a source/sink free region.[22] Spherical Hankel functions $(j = 1)$ are meanwhile used to describe the scattered field in the outer region. Within all other layers the field is represented as a superposition of $j = 1$ and $j = 2$ multipole contributions, which will in general be of differing strengths, to allow for transmission and reflection at each boundary. By applying Maxwell's boundary conditions at each interface (i.e., applying standard Mie theory), it can be shown that each multipole mode experiences a simple scaling in strength dependent only on its order, with no cross coupling, such that relations of the form,

$$a_{lm}^{\nu(3)} = \mathcal{G}_l^{\nu}b_{lm}^{\nu(1)} = \mathcal{H}_l^{\nu}c_{lm}^{\nu(3)}, \tag{3}$$

hold. Explicit forms of the scaling factors between mode weightings in each region, including $\mathcal{G}_l^{\nu}$ and $\mathcal{H}_l^{\nu}$, can be found in Ref. 26. It is however noted here that these factors depend on the material properties (via k_1 and k_2), illumination

wavelength, and the NP geometry only, but not on the illumination pattern. Evanescent coupling, as plays a key role in plasmonics, is accounted for via the complex nature of k_1 (and hence also k) within each region.

It is noted that in many practical arrangements, it becomes necessary to focus the illumination beam through materials of differing refractive indices. One such example is that of a sample mounted on a glass microscope slide and covered with a protective cover slip. Naturally, the presence of such a stratified media affects the focal distribution of light, a problem which has been addressed in the literature (e.g., Ref. 27). In particular, inclusion of a stratified sample structure predominantly leads to spherical aberration in the focused field distribution. This, in turn, does not change the symmetry of the focusing problem, albeit does change the effective multipole coefficients of the illumination seen by the NP. For the work presented in this article, a stratified sample structure is therefore not considered since, given the results of Ref. 27, it is evident that qualitatively our results are unaffected. Exact quantitative values of calculated enhancement factors will differ from the stratified case, however, assuming the refractive index mismatch is small (or zero in the case of an oil immersion lens in which the immersion oil is matched to the cover slip, in addition to the objective lens) the discrepancies will be small. Finally, the optical arrangement used for readout will also affect the measured signal. While full exposition of the resulting effects is beyond the scope of this article, the qualitative results of this work are again unaffected. The interested reader is directed to Refs. 28 and 29. A specific treatment of the high NA imaging of multipole modes is also given in Ref. 30.

B. Enhancement at the center of on-axis in-focus NPs

Consider first the simplest geometry of focusing an arbitrary beam onto an NP whose center is located at the geometric focal point of the illumination system. The electric field enhancement at a position $\mathbf{r}$ can then be defined, as per usual convention, as

$$\Gamma(\mathbf{r}) = \frac{|\mathbf{E}_{\text{NP}}(\mathbf{r})|^2}{|\mathbf{E}_{\text{no-NP}}(\mathbf{r})|^2}, \tag{4}$$

where $\mathbf{E}_{\text{NP}}(\mathbf{r})$ and $\mathbf{E}_{\text{no-NP}}(\mathbf{r})$ is the field with and without the NP, respectively. The latter is simply the focused field distribution as given by the first term of Eq. (2). Equation (4) describes the enhancement at a single point, and is hence an appropriate metric for, for example, single molecule spectroscopy, however, in other applications (e.g., fluorescence and nonlinear optics), it is more appropriate to consider an average of the field or higher powers thereof. Some results in this vein are given in Sec. II D.

Temporarily restricting attention to the enhancement within the core of the NP, as is pertinent to scenarios in which fluorescent emitters are embedded within the core of the NP,[8,9,31–38] means the enhancement can be written in the form,

$$\Gamma(\mathbf{r}) = \frac{\left|\sum_\nu \sum_{l,m} c_{lm}^{\nu(3)} \mathbf{E}_{lm}^{\nu(3)}(\mathbf{r})\right|^2}{\left|\sum_\nu \sum_{l,m} a_{lm}^{\nu(3)} \mathbf{E}_{lm}^{\nu(3)}(\mathbf{r})\right|^2}. \tag{5}$$

Additional simplifications follow by restricting further to the origin of the coordinate system (i.e., the focal point). Using the Maclaurin expansion of the spherical Bessel function,

$$h_l^{(3)}(z) = \frac{z^l}{(2l+1)!!}\left(1 - \frac{z^2}{2(2l+3)} + \cdots\right),$$

it is possible to show that the forms of the electric dipole fields ($l = 1$) at the origin are[39]

$$\mathbf{E}_{1,\pm1}^{E(3)}(\mathbf{0}) = \mp\frac{2k}{3}\left(\frac{3}{4\pi}\right)^{1/2}\frac{1}{\sqrt{2}}(\hat{\mathbf{x}} \pm \hat{\mathbf{y}}),$$

$$\mathbf{E}_{1,0}^{E(3)}(\mathbf{0}) = \frac{2k}{3}\left(\frac{3}{4\pi}\right)^{1/2}\hat{\mathbf{z}},$$

while all other multipole modes (magnetic dipole, electric quadrapole, etc.) are identically zero. Direct substitution then yields

$$\Gamma(\mathbf{0}) = \left|\frac{1}{\mathcal{H}_1^E}\frac{k_I}{k_N}\right|^2 = \left|\frac{1}{\mathcal{H}_1^E}\frac{\epsilon_I}{\epsilon_N}\right|^2. \tag{6}$$

The subscripts on k and ϵ denote the differing value within different media. It should be noted that the latter equality in Eq. (6) only holds for the case of nonconducting materials in regions I and N (as is generally the case). Similar results have been obtained by other authors[31,32,34,38] albeit in a somewhat different context.

Equation (6) shows that the enhancement factor at the geometric optics focal point is dependent on only the NP properties and illumination wavelength [i.e., $\Gamma(\mathbf{0})$ is independent of the illumination beam profile used]. Figure 3 shows the enhancement factor calculated via Eq. (6) for shell-core NPs immersed in water ($n = 1.33$) of different inner radii, r_I, ranging from 1 to 35 nm.[40] A silicon dioxide (SiO_2) core ($n = 1.46$) and a gold shell (refractive index data taken from Ref. 41) were assumed and the outer radius of the shell was fixed at $1.3r_I$. When compared with the enhancement factors predicted under a quasistatic approximation,[42] excellent

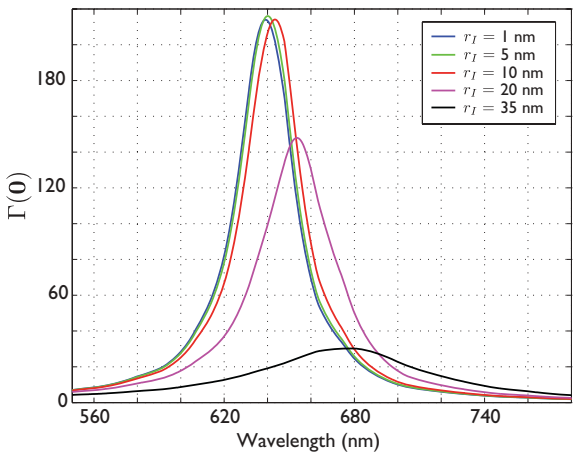

FIG. 3. (Color online) Theoretical enhancement factors at the center of a two-layer NP with a SiO_2 core and Au shell immersed in water, for different core radii r_I as a function of illumination wavelength. For small NPs good agreement with quasistatic predictions are found, however, this quickly breaks down as the NP dimensions are increased.

agreement is seen with the more rigorous Mie calculations for a 1-nm radius NP, however, discrepancies occur for NPs with radius $\gtrsim$10 nm.

Strictly, the illumination independence expressed in Eq. (6) requires the illumination field at the focus to be nonzero in the absence of the NP (i.e., $\mathbf{E}_{\text{no-NP}}(\mathbf{0}) \neq \mathbf{0}$), and hence is not applicable to a number of beams, notably azimuthally and circularly polarized LG beams. For this class of "dark spot" focal distributions the leading contribution to the illumination are the magnetic dipole (or potentially even higher order) terms, which have zero electric field at the origin. Mathematically, the enhancement in this case at the center of the NP can be found by taking the limit of Eq. (5) as $r \to 0$, yielding

$$\lim_{\mathbf{r}\to\mathbf{0}} \Gamma(\mathbf{r}) = \left| \frac{1}{\mathcal{H}_L^\mu} \frac{k_I}{k_N} \right|^2 = \left| \frac{1}{\mathcal{H}_L^\mu} \frac{\epsilon_I}{\epsilon_N} \right|^2, \tag{7}$$

where μ, L defines the leading order term in the focused beam. This result is, however, a mathematical singularity arising from the singularity in the electric field and hence has little physical consequence. It will in fact be seen shortly that the result of Eq. (6) can be restored for dark spot illuminations in reality.

C. Enhancement at the center of arbitrarily positioned NPs

The theory described thus far is formulated in terms of a coordinate system with its origin at the center of the NP. If, however, the NP is shifted away from the focal point of the illumination system (by $\mathbf{r}_{\text{NP}}$), as, for example, in scanning microscopy, the multipole representation used to describe the focused field, and that used to match the fields at the interface of the NP will no longer match. This complication can be considered by first defining two coordinate systems: one with its origin at the focal point of the illumination system in which positions are described by the vector $\mathbf{r}$; and one with the origin at the center of the shifted NP in which positions are described by the vector $\mathbf{r}' = \mathbf{r} - \mathbf{r}_{\text{NP}}$. Any field can be represented using multipole expansions in both of these coordinate systems. Therefore, consider representing a field in terms of vectorial multipoles centered on $\mathbf{r} = 0$ and $\mathbf{r}' = 0$, such that

$$\mathbf{E}(\mathbf{r}) = \sum_\nu \sum_{l,m} a_{lm}^{\nu(3)} \mathbf{E}_{lm}^{\nu(3)}(\mathbf{r}) = \sum_\mu \sum_{L,M} \alpha_{LM}^{\mu(3)} \mathbf{E}_{LM}^{\mu(3)}(\mathbf{r}').$$

Note that for the purposes of this article only the $j = 3$ modes need be considered. To relate the expansion coefficients $a_{lm}^{\nu(3)}$ and $\alpha_{LM}^{\mu(3)}$ in the two coordinate systems it is noted that

$$\mathbf{E}_{lm}^{E(3)}(\mathbf{r}) = \sum_{L,M} \mathcal{A}_{LM}^{lm} \mathbf{E}_{LM}^{E(3)}(\mathbf{r}') + \frac{k}{k_2} \mathcal{B}_{LM}^{lm} \mathbf{E}_{LM}^{M(3)}(\mathbf{r}'),$$

$$\mathbf{E}_{lm}^{M(3)}(\mathbf{r}) = \sum_{L,M} \mathcal{A}_{LM}^{lm} \mathbf{E}_{LM}^{M(3)}(\mathbf{r}') + \frac{k_2}{k} \mathcal{B}_{LM}^{lm} \mathbf{E}_{LM}^{E(3)}(\mathbf{r}'),$$

such that

$$\alpha_{LM}^{E(3)} = \sum_{l,m} \left(a_{lm}^{E(3)} \mathcal{A}_{LM}^{lm} + \frac{k_2}{k} a_{lm}^{M(3)} \mathcal{B}_{LM}^{lm} \right), \tag{9}$$

$$\alpha_{LM}^{M(3)} = \sum_{l,m} \left(a_{lm}^{M(3)} \mathcal{A}_{LM}^{lm} + \frac{k}{k_2} a_{lm}^{E(3)} \mathcal{B}_{LM}^{lm} \right). \tag{10}$$

Explicit forms of the transformation matrices $\mathcal{A}_{LM}^{lm}$ and $\mathcal{B}_{LM}^{lm}$ can be derived by virtue of the scalar addition theorem for the scalar spherical harmonics, and can be found in the work of Chew.[43]

As before the field enhancement can then be defined for an arbitrarily shifted NP by Eq. (4). Physically, it is equivalent to consider the enhancement factor in the shifted coordinate system such that

$$\Gamma(\mathbf{r}) = \frac{\left| \sum_\mu \sum_{L,M} \gamma_{LM}^{\mu(3)} \mathbf{E}_{LM}^{\mu(3)}(\mathbf{r}') \right|^2}{\left| \sum_\mu \sum_{L,M} \alpha_{LM}^{\mu(3)} \mathbf{E}_{LM}^{\mu(3)}(\mathbf{r}') \right|^2}, \tag{11}$$

where $\gamma_{LM}^{\mu(3)}$ are the multipole coefficients of the field inside the NP in the shifted coordinate system. $\gamma_{LM}^{\mu(3)}$ can be related to the coefficients $c_{lm}^{\nu(3)}$ via expressions analogous to Eqs. (9) and (10). Again, considering the enhancement at the center of the NP (i.e., $\mathbf{r} = \mathbf{r}_{\text{NP}}$, or equivalently $\mathbf{r}' = \mathbf{0}$) only the dipole terms in the shifted coordinate system need be considered. In the shifted coordinates, however, the multipole coefficients $\alpha_{LM}^{\mu(3)}$ and $\gamma_{LM}^{\mu(3)}$ are related via $\alpha_{LM}^{\mu(3)} = \mathcal{H}_L^\mu \gamma_{LM}^{\mu(3)}$ [c.f. Eq. (3)], such that

$$\Gamma(\mathbf{r}_{\text{NP}}) = \left| \frac{1}{\mathcal{H}_1^E} \frac{k_I}{k_N} \right|^2 = \left| \frac{1}{\mathcal{H}_1^E} \frac{\epsilon_I}{\epsilon_N} \right|^2, \tag{12}$$

where the latter equality again only holds for $\sigma_I = \sigma_N = 0$. Equation (12) demonstrates that even for off-axis illumination of the NP, the field enhancement is independent of the illumination beam profile. Formally, this latter claim requires $\alpha_{1M}^{E(3)} \neq 0$ for at least one value of M, such that $\mathbf{E}_{\text{no-NP}}(\mathbf{r}' = \mathbf{0}) \neq \mathbf{0}$, however, from Eq. (9) it is evident that $\alpha_{1M}^{E(3)}$ has contributions from all nonshifted multipole modes in the illumination beam, such that this requirement is likely to be satisfied in most cases. In this way, it is further seen that while the on-axis result of Eq. (6) did not apply to all beam profiles, infinitesimal shifts of the NP, or the presence of any small perturbation, for example, noise, in the illumination beam, restores the illumination independence of the enhancement factor. It is emphasized here, that for the complex beams under consideration, the field impinging on the NP can vary on a scale comparable to the size of the NP, even in the electrostatic limit. A good example is that of a LG_{01} beam where the focused field changes sign over the dimensions of the NP. In this case the illumination field has a different symmetry than that usually assumed in a plane-wave illumination, such that the illumination independence found here is nontrivial.

Interestingly, as a brief aside, it should be noted that due to the symmetry breaking that arises when shifting the NP in relation to the focused field, a nonzero electric field results at $\mathbf{r} = \mathbf{0}$, even for dark spot type illuminations. Given that the electric field of such illumination fields is, however, unchanged (i.e., is still identically zero), locally an infinite enhancement is seen. This is merely a result of the definition of enhancement factor and is not a physical effect.

To confirm Eqs. (6) and (12) full Mie scattering calculations were performed to determine the field at the center of a shifted shell-core NP under differing illumination conditions. Solution of the scattering problem was discussed above and, given the scaling coefficients $\mathcal{G}_l^\nu$, $\mathcal{H}_l^\nu$, etc., reduces to determination

TABLE I. Parameter values for illumination beams used in numerical simulations.

	$\widetilde{E}(\theta)$	p	n	ϕ_0
Laguerre-Gaussian (LG_{ab})	Eq. (14)	0	b	0
Radial polarization	1	1	0	0
Azimuthal polarization	1	1	0	$-\frac{\pi}{2}$

of the appropriate multipole weightings $a_{lm}^{\nu(3)}$ for a given illumination. A general solution for arbitrary illumination profiles exists,[22] however a restricted class of cylindrically polarized vortex beams is considered here, merely to enable use of a semianalytic solution. This restriction does not reflect a limitation of the results presented in this work. Cylindrically polarized vortex beams can be defined in the pupil of the illumination lens by the generalized Jones vector,

$$\begin{bmatrix}\widetilde{E}_x^{\mathrm{col}}(\theta,\phi)\\ \widetilde{E}_y^{\mathrm{col}}(\theta,\phi)\end{bmatrix} = \begin{bmatrix}\cos(p\phi+\phi_0)\\ \sin(p\phi+\phi_0)\end{bmatrix}\widetilde{E}(\theta)e^{in\phi} \tag{13}$$

[neglecting the zero $\widetilde{E}_z^{\mathrm{col}}(\theta,\phi)$ component], where (θ,ϕ) are the usual spherical polar angles which define the direction of propagation of individual rays originating from the pupil,[22] $\widetilde{E}(\theta)$ describes the amplitude variation across the beam profile, $n\in\mathbb{Z}$ is the topological charge, $p\in\mathbb{Z}$ is the cylindrical vector order, and ϕ_0 is a phase constant. The values of these parameters for the beams considered here, specifically x-polarized LG_{00}, x-polarized LG_{01}, radially polarized and azimuthally polarized beams, are shown in Table I.

The LG beams were assumed to be defined using

$$\widetilde{E}(\theta) = E_{ab}\, s^{|b|}\exp(-s^2)L_a^b(2s^2), \tag{14}$$

where $s=\sin\theta/w_0$, E_{ab} is a mode dependent constant, w_0 is the beam waist (measured in focal lengths and fixed at a value of 0.9 for all calculations) assumed to be located in the exit pupil of the lens, and $L_a^b(x)$ are the Laguerre polynomials. The nonzero mode weighting coefficients for these beams can then be shown to be given by

$$a_{l,m_\pm}^{E(3)} = \frac{e^{\pm\phi_0}}{i^l}\frac{4\pi\, C_{l,m_\pm}}{l(l+1)}\int_0^{\Psi} a(\theta)\widetilde{E}(\theta)\Theta_{l,m_\pm}^{\mp}(\theta)\sin\theta d\theta, \tag{15}$$

for $p\neq 1$ (e.g., focused x-polarized LG beams) where $m_\pm = n\pm p\mp 1$, Ψ is the half angle of convergence of the lens,

$$\Theta_{l,m}^{\pm}(\theta) = \left[\frac{\partial}{\partial\theta}P_l^{|m|}(\cos\theta)\pm\frac{m}{\sin\theta}P_l^{|m|}(\cos\theta)\right], \tag{16}$$

and $a(\theta)$ is an apodization factor required to conserve energy ($=\sqrt{\cos\theta}$ for an aplanatic lens). The magnetic multipole contributions are given by the relation $a_{l,m_\pm}^{E(3)} = \pm(k_2/k)\,a_{l,m_\pm}^{M(3)}$. For the $p=1$ case (i.e., radially and azimuthally polarized beams),

$$\begin{aligned}a_{l,n}^{\nu(3)} = {}& \frac{4\pi\, C_{l,n}}{i^l\, l(l+1)}\left(\delta_{\nu E}-\frac{k}{ik_2}\delta_{\nu M}\right)\\ &\times\int_0^{\Psi} a(\theta)\widetilde{E}(\theta)\left[e^{i\phi_0}\Theta_{l,n}^{-}(\theta)+(-1)^{\delta_{\nu M}}e^{-i\phi_0}\Theta_{l,n}^{+}(\theta)\right]\\ &\times\sin\theta d\theta,\end{aligned} \tag{17}$$

where $\delta_{\nu\mu}$ is the Kronecker delta. Nanoparticle displacements from 0 to 100 nm were considered and the focusing lens was assumed to have a numerical aperture (NA) of 1.2 (including the immersion effect of the water). Transformation matrices $\mathcal{A}_{LM}^{lm}$ and $\mathcal{B}_{LM}^{lm}$ were implemented using recursive relations found in the literature.[44–46] Numerical evaluation of the resulting enhancement factor yields plots identical to those of Fig. 3 regardless of illumination beam profile and displacement size (not shown to avoid repetition).

D. Effective enhancements near the surface of a NP

For many applications it is the enhancement close to the surface of the NP (in region N) that is more relevant than that within the core.[21,47–49] In this case the numerator of Eq. (4) becomes

$$\left|\sum_{\nu}\sum_{l,m} a_{lm}^{\nu(3)}\mathbf{E}_{lm}^{\nu(3)}(\mathbf{r}) + b_{lm}^{\nu(3)}\mathbf{E}_{lm}^{\nu(1)}(\mathbf{r})\right|^2, \tag{18}$$

while the denominator remains unchanged. As a result of the higher order multipole contributions (e.g., magnetic dipole terms) present in the illumination beam, and the different scaling coefficients for each, a dependence on the illumination beam profile is introduced. Even in the case when only electric dipole illumination is used (see, e.g., Ref. 50) the position dependence of the individual dipole modes can give rise to different enhancement distributions. For example, the electric dipole terms are strongest for both a focused x-polarized LG_{00} and LG_{01} beam, yet inspection of the full enhancement maps for scattering from a homogeneous 2-nm radius Au sphere [as shown in the x-z plane in Figs. 4(a) and 4(b), respectively] reveals a clear directionality. In particular this directionality arises from dominance of different m modes in each case: For the focused LG_{00} beam the $m=0$ electric dipole mode (representing a dipole with moment oriented parallel to the z axis) is absent, while for the LG_{01} case the $m=0$ is the only electric dipole contribution present.

Useful signal is, however, frequently not generated by a single point. For example, coatings of fluorescent molecules have been placed over spherical NPs,[51] such that the measured fluorescence signal originates from the entire NP surface. Consideration of the enhancement of the integrated intensity (or what shall be termed the effective enhancement), defined

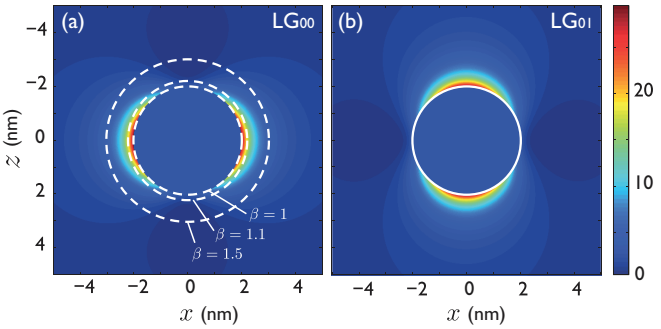

FIG. 4. (Color online) Maps of the near-field enhancement $\Gamma(\mathbf{r})$ for scattering from a 2-nm radius homogenous Au NP illuminated by a focused x-polarized LG_{00} (a) and LG_{01} beams (b). White dashed lines in (a) represent the fixed radii at which the effective enhancement is calculated in Fig. 5 as defined by $r=\beta r_I$ for $\beta=1$,1.1 and 1.5.

as

$$\widetilde{\Gamma}(r) = \frac{\int_0^{2\pi}\int_0^{\pi} |\mathbf{E}_{\mathrm{NP}}(\mathbf{r})|^2 \sin\vartheta\, d\vartheta\, d\varphi}{\int_0^{2\pi}\int_0^{\pi} |\mathbf{E}_{\text{no-NP}}(\mathbf{r})|^2 \sin\vartheta\, d\vartheta\, d\varphi}, \tag{19}$$

is consequently more pertinent. $\widetilde{\Gamma}(r)$ can also be evaluated above the surface of the NP, as may be appropriate for coatings of molecules with a finite thickness or for fluorophores placed a (small) distance away from the surface to avoid quenching.[21] A similar effective enhancement can also be defined if the detected signal originated from a finite volume, whereby surface integrals in Eq. (19) would be replaced by volume integrals. Orthogonality of the multipole modes over a spherical surface, and Eq. (3), allows Eq. (19) to be simplified yielding

$$\widetilde{\Gamma}(r)=1+\frac{\sum_\nu\sum_{l,m}\left|a_{lm}^{\nu(3)}/\mathcal{G}_l^\nu\right|^2\left[I_{l,N}^{\nu(1,1)}(r)+2\mathrm{Re}\left\{\mathcal{G}_l^\nu I_{l,N}^{\nu(3,1)}(r)\right\}\right]}{\sum_\nu\sum_{l,m}\left|a_{lm}^{\nu(3)}\right|^2 I_{l,N}^{\nu(3,3)}(r)}, \tag{20}$$

where Re denotes the real part and

$$I_{l,N}^{M(i,j)}(r) = l(l+1)|k_{2,N}|^2 h_l^{(i)}(k_N r) h_l^{(j)*}(k_N r), \tag{21}$$

$$I_{l,N}^{E(i,j)}(r) = \frac{l(l+1)}{r^2}\left[\frac{I_{l,N}^{M(i,j)}(r)}{|k_{2,N}|^2} + \frac{d}{dr}\left(r h_l^{(i)}(k_N r)\right)\frac{d}{dr}\left(r h_l^{(j)*}(k_N r)\right)\right]. \tag{22}$$

If in any scenario the $\nu = \mu$ and $l = L$ modes are dominant (e.g., if only electric dipole terms are present $\mu = E$ and $L = 1$), Eq. (20) reduces to

$$\widetilde{\Gamma}(r) = 1 + \frac{I_{L,N}^{\mu(1,1)}(r) + 2\mathrm{Re}\left[\mathcal{G}_L^\mu I_{L,N}^{\mu(3,1)}(r)\right]}{\left|\mathcal{G}_L^\mu\right|^2 I_{L,N}^{\mu(3,3)}(r)}, \tag{23}$$

which is independent of the illumination coefficients $a_{lm}^{\nu(3)}$ and hence the exact form of the beam profile. The dominant mode, however, need not be the electric dipole terms. For example, for illumination by a focused azimuthally polarized beam, the dominant modes are magnetic dipoles for which Eq. (23) would still hold with $\mu = M$ and $L = 1$. The equivalent results for signal collection from a spherical shell takes the same form of Eqs. (20) and (23), with the replacement $I_{l,N}^{\nu(i,j)}(r) \to \int_{R_1}^{R_2} I_{l,N}^{\nu(i,j)}(r) r dr$, where R_1 and R_2 define the inner and outer radius of the shell, respectively.

To investigate the effective enhancement factor further, $\widetilde{\Gamma}(r)$ was calculated for scattering from a single NP under a variety of scenarios (see Fig. 5). In all cases a single Au NP immersed in water and with its center located at the geometrical focus of the illuminating lens was taken. This NP geometry was adopted due to the common use of such NPs. First, the effective enhancement at an infinitesimal distance above the surface of the NP (i.e., at $r = \beta r_I$ with $\beta = 1$) was determined as the radius of the NP was varied over the range $0 < r_I \leqslant 100$ nm. Consider first the case of scattering when the NP is illuminated by a focused LG_{00} beam (vacuum wavelength of 533 nm and NA of 1.2 including the immersion effect of the water were assumed) as represented by the uppermost blue curve in Fig. 5(a). A peaked distribution

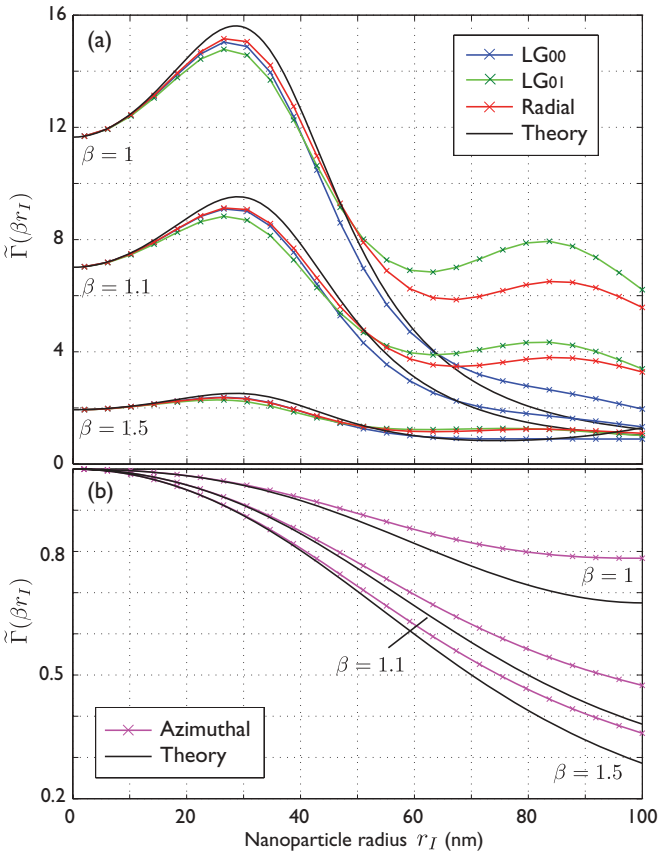

FIG. 5. (Color online) Colored lines with data points show the variation of the calculated effective enhancements $\widetilde{\Gamma}(r)$ at fixed radii above the surface of an Au NP, as its radius is varied. White dashed lines in Fig. 4(a) represent the fixed radii at which the effective enhancement is calculated as defined by $r = \beta r_I$ for $\beta = 1, 1.1$ and 1.5. Different colored lines represent different illumination beams as follows: (blue) LG_{00}, (green) LG_{01}, (red) radial polarization, and (purple) azimuthal polarization (shown in a separate panel for clarity). Black solids lines represent the effective enhancement as predicted by Eq. (23) for electric dipole terms only (top panel) and magnetic dipole terms only (bottom panel).

is seen as the NP dimensions are varied (the illumination wavelength was selected so as to lie close to the resonance predicted by quasistatic theory), with the peak occurring at radius of $r_I \approx 27$ nm. Naturally the position of this peak will vary with the illumination wavelength as would be expected from its plasmonic origin (cf. Fig. 3). Given that a focused LG_{00} beam has relatively strong (albeit not entirely dominant) electric dipole contributions, reasonable agreement would be expected with the predictions of Eq. (23) with $\mu = E$ and $L = 1$. This electric dipole only approximation is depicted by the uppermost solid black curve of Fig. 5(a). Indeed this expectation is born out in simulations. Generally the differences between the full calculations and the electric dipole only approximation increase as the NP radius increases. This behavior is to be expected since for larger NPs scattering of high order terms plays more of a role, as also predicted by standard Mie theory for plane-wave illumination.[24]

If a focused LG_{01} or radial polarized beam is used to illuminate the NP similar results to the LG_{00} case are seen

for small NPs [uppermost green and red curves of Fig. 5(a), respectively]. Since magnetic dipole and higher order terms are relatively stronger in these beams than in a LG_{00} beam, the divergences from Eq. (23) are, however, more severe at larger NP sizes. It should be noted that the electric dipole approximation in these cases breaks down at smaller NP dimensions than the 100 nm quoted for a focused x-polarized beam,[52] solely due to the differing illumination conditions. Again it is emphasized that variations of the focal field can occur over subwavelength scales. For the case of a focused azimuthal polarized beam, as shown by the purple curves in Fig. 5(b), the electric dipole theory completely breaks down since the illumination beam contains only magnetic dipole (and higher order) components. As such, use of Eq. (23) with $\mu = M$ and $L = 1$ [uppermost black curve of Fig. 5(b)], produces good agreement with the nonapproximate calculations. Differences again begin to arise at larger NP dimensions. Comparison of this observation with that of Eq. (12) might be said to produce a logical contradiction, since Eq. (12) shows that the enhancement at the center of the NP is determined by the electric dipole terms. No contradiction exists, however, because the specific symmetry inherent to the center of the NP [i.e., where Eq. (12) is valid] implies that all but the electric dipole terms have zero electric field such that higher orders play no formal role at all. When considering the enhancement over a sphere, however, all multipole terms must be considered and therefore it is the strongest modes in the illumination that dominate the behavior of the enhancement ratio.

Performing the analogous calculations of the effective enhancement at different radii above the NP surface produces qualitatively similar results to those seen when $\widetilde{\Gamma}$ was calculated at the NP surface. Specifically, the effective enhancement was also calculated at $r = \beta r_I$ with $\beta = 1.1$ and 1.5, as depicted by the dashed white circles in Fig. 4(a). The corresponding families of curves are also shown in Fig. 5. While the form of the resulting curves are similar (although not exactly the same) a clear reduction in the overall enhancement factor is seen at larger distances from the NP arising by virtue of the evanescent nature of the near field.

Enhancement factors defined in terms of higher orders of the electric field can also be constructed. For example, if looking at the plasmonic enhancement of two photon fluorescence, an effective enhancement defined analogously to Eq. (19), albeit with the replacement $|\mathbf{E}(\mathbf{r})|^2 \rightarrow |\mathbf{E}(\mathbf{r})|^4$ would be more appropriate. Indeed, numerical calculations have also been performed in this vein, under the same conditions as the calculations of Fig. 5. A similar functional dependence on NP radius and numerical aperture was seen, albeit numerical values of the effective enhancement differed greatly from those of Fig. 5. For example, for a LG_{00} illumination the peak effective enhancement (for $\beta = 1$) was seen for $r_I \approx 27$ nm, as also seen in Fig. 5, however, the peak enhancement took a value of $\approx$330. Analytical results, unfortunately, are not easily obtainable in this case, however due to the amplifying effect of taking higher exponents of the field, a greater dependence of the enhancement factor on illumination profile would be expected. This is indeed seen in simulations.

As a final study, the dependence of the effective enhancement factor on the NA of the illumination lens was considered. Again scattering from a single Au sphere in water under different illuminations (of wavelength 533 nm) was considered. While the effective enhancement was only considered at the NP surface, three different sized NPs were modeled ($r_I = 2, 30, 100$ nm). The results are shown in Fig. 6. For reference the thick vertical dashed line shows the NA corresponding to the calculations of Fig. 5. The first point to note in Fig. 6 is that for a 2-nm radius NP (solid lines, which are coincident for all illumination cases considered, except azimuthal polarization), the effective enhancement factor is independent of illumination NA, remaining constant at a value just below 12. Low NA illumination optics approximately corresponds to illumination of the NP by a plane wave, such that for 2-nm NPs the quasistatic approximation is valid. Given that the effective enhancement remains constant, it can be concluded that the quasistatic approximation holds for all numerical apertures, if the NP is small enough. Moving to larger NPs it is seen that a variation with NA is introduced, indicating that the quasistatic approximation breaks down and higher order multipole modes begin to play a more dominant role. That said for practical NP sizes of $\sim$30 nm this effect is weak with the differences over an NA range of 1.3 accounting for less than 1 part in 15 variation in $\widetilde{\Gamma}$.

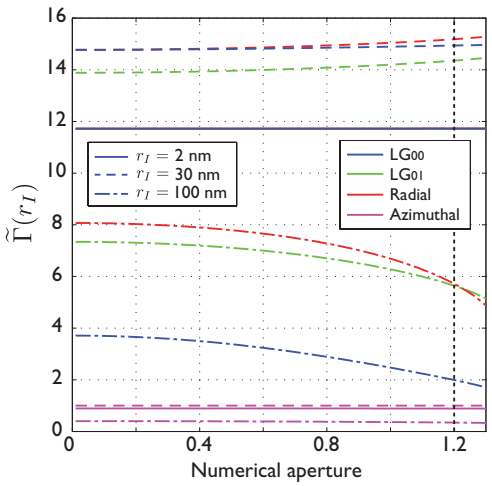

FIG. 6. (Color online) Variation of effective enhancement factor $\widetilde{\Gamma}$ as a function of NA of the illumination lens. $\widetilde{\Gamma}$ has been evaluated at the surface of differently sized homogeneous Au NPs for differing focused beam profiles (see text) and NP dimensions. Illumination wavelength was fixed at 533 nm.

In the interests of completeness it is worthwhile to mention the behavior of the effective enhancement when the NP is shifted away from the focal point. Similar results to the on-axis case can be found, however, by virtue of the multipole shift equations it is unlikely that any one class of multipoles will be dominant in the illumination field seen by the NP. Consequently, exact illumination independence will not hold. If, however, the NP radius, or the magnitude of the displacement, is small in comparison to the wavelength, only a weak dependence would be expected.

III. CONCLUSIONS

In summary, this article has considered the dependence of plasmonic near-field enhancements of spherical NPs on the

illumination field incident upon them. For this geometry it has been possible to derive a general result, namely that at the center of an NP the field enhancement factor is independent of the illumination profile. This result holds true for a particle of spherical symmetry, irrespective of the number of layers, material properties, NP dimensions, and precise position of the NP within the illumination pattern. This is an exact result and relies on no approximations. Numerical values of the enhancement factor depend solely on the properties of the immersion medium and NP, such as size and composition via Eq. (12). Relaxation of the assumption of NPs with spherical symmetry, implies cross coupling between multipole modes occurs at each interface of the NP, and thus formally invalidates the exact illumination independence found, however, for small (in the sense that the quasistatic limit holds) NPs the strength of mixing will be weak, thus preserving the illumination independence in an approximate sense for arbitrary NP shapes. The NP geometry will again, however, affect the numerical values of enhancement obtained in this case. Given this result it is, however, important to note that while enhancement ratios at the NP core have been shown to be independent of the illumination structure, the absolute value of the local field, and hence also the intensity, is not. Indeed if a field of maximum intensity is sought at the center of an on-axis in-focus NP, pure electric dipole illumination fields should be used.[50] While an electric dipole illumination field has a spherical wavefront (as would be expected for a focused wave), the amplitude and polarization distributions across the pupil are nonuniform. If maximum intensity is sought off-axis then only an electric dipole mode in the shifted coordinate system centered on the relevant off-axis point (c.f. Sec. II C) must be present. The associated illumination beam (which will possess higher order multipole modes) can then be inferred using inverse multipole shift formulas, derivable from Eqs. (9) and (10).

Moving beyond consideration of enhancements within the core of NPs, an effective enhancement factor for average enhancements over spherical surfaces (and volumes) was defined and investigated. Specifically, it was further shown that this effective enhancement can also exhibit illumination independent behavior. For example, exact illumination independence is seen if one class of multipole modes only is present in the illumination beam. Approximate independence is seen if one class of modes is dominant. In particular the dependence of the effective enhancement factor on illumination becomes more apparent for larger NP sizes and illumination NA. The latter effect was, however, demonstrated to be a fairly weak one. While not explicitly considered in this text, an average enhancement could be defined within the core (or intermediate layers) of an NP. The uniformity of the enhancement for on-axis in-focus NPs [see, e.g., Fig. 5(a)], imply that these will be numerically similar to the enhancement obtained at the origin. This is, however, likely to break down for dark spot type illuminations and shifted NPs, however fuller investigation remains as future work.

The results presented in this article enable substantial simplification of numerical calculations of near-field enhancements when complicated illumination beams are used. Full calculations can often require development of complex code and increased simulation times, however, the results here show that under many circumstances it is reasonable, and accurate, to use a plane-wave illumination.

ACKNOWLEDGMENTS

M.R.F. acknowledges financial support from the Engineering and Physical Sciences Research Council. Y.S. acknowledges support from the European Science Foundation, and thanks Y. Sonnefraud and A. I. Fernández-Domínguez for many useful discussions.

*matthew.foreman@imperial.ac.uk

[1] V. Giannini, A. I. Fernández-Domínguez, S. C. Heck, and S. A. Maier, Chem. Rev. **111**, 3888 (2011).
[2] M. G. L. Gustafsson, Proc. Natl. Acad. Sci. USA **102**, 13081 (2005).
[3] F. Wei and Z. Liu, Nano Lett. **10**, 2531 (2010).
[4] H. Zhang, M. Zhao, and L. Peng, Opt. Express **19**, 24783 (2011).
[5] S. W. Hell and J. Wichmann, Opt. Lett. **19**, 780 (1994).
[6] T. Klar, S. Jakobs, M. Dyba, A. Egner, and S. W. Hell, Proc. Nat. Acad. Sci. USA **97**, 8206 (2000).
[7] P. Török and P. R. T. Munro, Opt. Express **12**, 3605 (2004).
[8] Y. Sivan, Y. Sonnefraud, S. Kéna-Cohen, J. B. Pendry, and S. A. Maier, ACS Nano **6**, 5291 (2012).
[9] Y. Sivan, Appl. Phys. Lett. **101**, 021111 (2012).
[10] F. Balzarotti and F. D. Stefani, ACS Nano **6**, 4580 (2012).
[11] D. Lim, T. N. Ford, K. K. Chu, and J. Mertz, J. Biomed. Opt. **16**, 016014 (2011).
[12] G. Volpe, S. Cherukulappurath, R. J. Parramon, G. Molina-Terriza, and R. Quidant, Nano Lett. **9**, 3608 (2009).
[13] G. Volpe, G. Molina-Terriza, and R. Quidant, Phys. Rev. Lett. **105**, 216802 (2010).
[14] N. Bokor and N. Davidson, Opt. Commun. **270**, 145 (2007).
[15] W. Chen and Q. Zhan, Opt. Commun. **265**, 411 (2006).
[16] G. M. Lerman, A. Yanai, N. Ben-Yosef, and U. Levy, Opt. Express **18**, 10871 (2011).
[17] J. Scheuer, Opt. Express **19**, 25454 (2011).
[18] B. Gjonaj, J. Aulbach, P. M. Johnson, A. P. Mosk, L. Kuipers, and A. Lagendijk, Nat. Phot. **5**, 360 (2012).
[19] J. A. Gordon and R. W. Ziolkowsky, Opt. Express **15**, 2622 (2007).
[20] A. Alù and N. Engheta, Phys. Rev. Lett. **100**, 113901 (2008).
[21] F. Tam, G. P. Goodrich, B. R. Johnson, and N. J. Halas, Nano Lett. **7**, 496 (2007).
[22] M. R. Foreman and P. Török, J. Mod. Opt. **58**, 339 (2010).
[23] C. J. R. Sheppard and P. Török, J. Mod. Opt. **44**, 803 (1997).
[24] M. Born and E. Wolf, *Principles of Optics*, 7th ed. (Cambridge University Press, Cambridge, 1980).
[25] N. J. Halas, Opt. Photon. News August 26 (2002).
[26] D. W. Mackowski, R. A. Altenkirch, and M. P. Menguc, Appl. Opt. **29**, 1551 (1990).
[27] P. Török and P. Varga, Appl. Opt. **36**, 2305 (1997).
[28] O. Haeberlé, M. Ammar, H. Furukawa, K. Tenjimbayashi, and P. Török, Opt. Express **11**, 2964 (2003).

[29]P. Török, P. R. T. Munro, and E. Kriezis, Opt. Express **16**, 507 (2008).
[30]M. R. Foreman and P. Török, New J. Phys. **13**, 063041 (2011).
[31]J. Enderlein, Appl. Phys. Lett. **80**, 315 (2002).
[32]J. Enderlein, Phys. Chem. Chem. Phys. **4**, 2780 (2002).
[33]Y. G. Sun and Y. N. Xia, Analyst **128**, 686 (2003).
[34]H. Xu, Phys. Rev. B **72**, 073405 (2005).
[35]X. Miao, I. Brener, and T. S. Luk, J. Opt. Soc. Am. B **27**, 1561 (2010).
[36]S. Zaiba, F. Lerouge, A.-M. Gabudean, M. Focsan, J. Lermé, T. Gallavardin, O. Maury, C. Andraud, S. Parola, and P. L. Baldeck, Nano Lett. **11**, 2043 (2011).
[37]W. Li, J. Zhang, Y. Zhoub, and P. Zhang, Chem. Commun. **47**, 5834 (2011).
[38]M. Klopfer and R. K. Jain, Opt. Mat. Exp. **1**, 1353 (2011).
[39]I. M. Bassett, Opt. Acta **33**, 279 (1986).
[40]For particle sizes of the order of a few nanometers, it is noted that quantum effects become important and should realistically be considered for an accurate description, however, these are neglected in this work for simplicity.
[41]E. D. Palik, ed., *Handbook of Optical Constants of Solids* (Academic Press, New York, 1985).
[42]S. Maier, *Plasmonics: Fundamentals and Applications* (Springer, New York, 2007).
[43]W. C. Chew, *Waves and Fields in Inhomogeneous Media* (IEEE Press, New York, 1995).
[44]W. C. Chew, J. Electromagnet. Wave **6**, 133 (1992).
[45]K. T. Kim, IEEE T. Antenn. Propag. **44**, 1482 (1996).
[46]Y. M. Wang and W. C. Chew, IEEE AP-S **1**, 174 (1993).
[47]P. L. Stiles, J. A. Dieringer, N. C. Shah, and R. P. Van Duyne, Ann. Rev. Anal. Chem. **1**, 601 (2008).
[48]M. A. Santiago-Cordoba, S. V. Boriskina, F. Vollmer, and M. C. Demirel, Appl. Phys. Lett. **99**, 073701 (2011).
[49]S. Kéna-Cohen, A. Wiener, Y. Sivan, P. N. Stavrinou, D. D. C. Bradley, A. Horsfield, and S. A. Maier, ACS Nano **5**, 9958 (2011).
[50]N. J. Moore, M. Alonso, and C. J. R. Sheppard, J. Opt. Soc. Am. A **24**, 3115 (2007).
[51]T. Matsuya, S. Tashiro, N. Hoshino, N. Shibata, Y. Nagasaki, and K. Kataoka, Anal. Chem. **75**, 6124 (2003).
[52]N. Mojarad, G. Zumofen, V. Sandoghdar, and M. Agio, J. Europ. Opt. Soc. Rap. Public. **4**, 09014 (2009).